



Deposited via The University of Sheffield.

White Rose Research Online URL for this paper:

<https://eprints.whiterose.ac.uk/id/eprint/236777/>

Version: Published Version

Article:

Teixeira, E.M., Poulot, G., van de Bruck, C. et al. (2026) Alleviating cosmological tensions with a hybrid dark sector. *Physical Review D*, 113 (2). 023514. ISSN: 2470-0010

<https://doi.org/10.1103/9lf2-33zf>

Reuse

This article is distributed under the terms of the Creative Commons Attribution (CC BY) licence. This licence allows you to distribute, remix, tweak, and build upon the work, even commercially, as long as you credit the authors for the original work. More information and the full terms of the licence here:
<https://creativecommons.org/licenses/>

Takedown

If you consider content in White Rose Research Online to be in breach of UK law, please notify us by emailing eprints@whiterose.ac.uk including the URL of the record and the reason for the withdrawal request.



Alleviating cosmological tensions with a hybrid dark sector

Elsa M. Teixeira^{1,*}, Gaspard Poulot^{2,†}, Carsten van de Bruck^{2,‡},
Eleonora Di Valentino^{2,§} and Vivian Poulin^{1,||}

¹*Laboratoire Univers et Particules de Montpellier, CNRS & Université de Montpellier (UMR-5299),
34095 Montpellier, France*

²*School of Mathematical and Physical Sciences, University of Sheffield,
Hounsfield Road, Sheffield S3 7RH, United Kingdom*



(Received 19 February 2025; accepted 1 December 2025; published 9 January 2026)

We investigate a cosmological model inspired by hybrid inflation, where two scalar fields representing dark energy (DE) and dark matter (DM) interact through a coupling that is proportional to the DE scalar field $1/\phi$. The strength of the coupling is governed solely by the initial condition of the scalar field, ϕ_i , which parametrizes deviations from the standard Λ cold dark matter (Λ CDM) model. In this model, the scalar field tracks the behavior of DM during matter domination until it transitions to DE while the DM component decays quicker than standard CDM during matter domination, and is therefore different from some interacting DM-DE models which behave like phantom dark energy. Using *Planck* 2018 CMB data, Dark Energy Spectroscopic Instrument baryonic acoustic oscillations measurements and Pantheon + supernova observations, we find that the model allows for an increase in H_0 that can help reduce the Hubble tension. In addition, we find that higher values of the coupling parameter are correlated with lower values of ω_m , and a mild decrease of the weak-lensing parameter S_8 , potentially relevant to address the S_8 tension. Bayesian model comparison, however, reveals inconclusive results for most datasets, unless SH_0 ES data are included, in which case a moderate evidence in favor of the hybrid model is found.

DOI: 10.1103/91f2-33zf

I. INTRODUCTION

Cosmological observations and models predict the existence of a dark sector. That is, cosmology requires additional degrees of freedom beyond the fields and particles of the standard model of particle physics. These new degrees of freedom dominate the Universe's energy budget today and are commonly known as dark matter (DM) and dark energy (DE). Dark matter is essential for structure formation. Because, as far as we know, it interacts with the standard model fields only via gravity, DM overdensities collapse and act as the first seeds for the formation of structures such as galaxies and galaxy clusters. On the other hand, the role of DE is to explain the accelerated expansion of the Universe at the present epoch, and it is so far compatible

with a perfectly homogeneous fluid. Cosmologists have developed an excellent working model of the Universe to explain various data, from the cosmic microwave background (CMB) anisotropies to the distribution of matter at large scales. It is encapsulated by the Λ cold dark matter (Λ CDM) model, in which DM is a cold, nonrelativistic fluid, and DE is portrayed by the cosmological constant Λ of general relativity. This model is a remarkable success story, explaining the overall properties of the Universe [1].

Despite these successes, there are good reasons to look beyond the Λ CDM model. The first reason is theoretical. Although scientists have developed models for DM and DE, the nature of the dark sector is still not understood. Dark matter might be weakly interacting massive particles or light scalar fields such as axions [2–4]. Dark energy might be the manifestation of a nonvanishing cosmological constant; nevertheless, it is essential to understand why this constant is so small compared to other energy scales in particle physics [5,6]. Until there is a solid theoretical foundation for DE and DM, cosmologists should continue investigating the theoretical foundations of the Λ CDM model.

The second reason to look beyond the Λ CDM model comes from observations. One of the most important open problems in cosmology is the persisting *Hubble tension* [7,8], a disagreement in the measurement of the current expansion rate of the Universe, H_0 , between late-time and

*Contact author: elsa.teixeira@umontpellier.fr

†Contact author: gmpoulot1@sheffield.ac.uk

‡Contact author: c.vandebruck@sheffield.ac.uk

§Contact author: e.divalentino@sheffield.ac.uk

||Contact author: vivian.poulin@umontpellier.fr

early-time observations from various cosmological probes (see, e.g., [9,10] for a review). Most notably, local observations by the SH_0 ES collaboration using absolutely calibrated Type-Ia supernovae find $H_0 = 73 \pm 1 \text{ km/s/Mpc}$ [11–13] (see also [14–29] for recent local measurement). On the other hand, the *Planck* Collaboration infers, from measurements of the CMB temperature and polarization anisotropies' angular power spectra, a value of $H_0 = 67.4 \pm 0.5 \text{ km/s/Mpc}$ [30], when the Λ CDM model is assumed in the analysis, in agreement with the recent ground based CMB estimates [31,32]. This tension exceeds 5σ significance and has provoked heated debates in the cosmology community about whether this difference could be due to systematic errors or whether it is a signal of new physics beyond Λ CDM [33–40].

Another tension, albeit with less statistical significance, pertains to the S_8 parameter, $S_8 \equiv \sigma_8 \sqrt{\Omega_m/0.3}$, where σ_8 is the variance of the matter density field at 8 Mpc scales and Ω_m is the fractional matter density. The S_8 *tension* refers to a mismatch in measurements of matter density fluctuations today as inferred from the CMB and galaxy surveys, see, e.g., [41–47]. Because of these theoretical and observational shortcomings, one needs to remain mindful that the Λ CDM model might only be a very good approximation for describing the Universe. We refer to [9,48] for an overview of current observational tensions and to [49] for a review of the suggested solutions to the Hubble tension.

In this work, we explore a model for the dark sector where DM and DE share a common origin in terms of two interacting scalar fields. Inspired by hybrid inflation and initially proposed in [50], this hybrid model introduces one additional parameter compared to the Λ CDM framework: the initial value of the DE field. This parameter governs the coupling strength between DM and DE, mediating the energy transfer from the DM fluid to the DE field. This interaction modifies the expansion history and offers a potential resolution to the Hubble and S_8 tensions while aligning with recent preferences for dynamical dark energy [51–58]. In this study, we constrain the hybrid model using current cosmological data, assuming adiabatic initial conditions for the cosmological perturbations.

The paper is organized as follows. After introducing the model in Sec. II, we detail the methodology followed in this analysis and present and discuss the results in Sec. III. We conclude our work in Sec. IV, where we also present an outlook for future directions of investigation.

II. THE HYBRID MODEL FOR THE DARK SECTOR

The model we consider is an interacting scalar field model inspired by hybrid inflation [59], described by the following action:

$$S = \int d^4x \sqrt{-g} \left[\frac{1}{2} M_{\text{Pl}}^2 R - \frac{1}{2} (\partial\phi)^2 - \frac{1}{2} (\partial\chi)^2 - V(\phi, \chi) \right] + S_{\text{SM}}, \quad (1)$$

where S_{SM} is the action of the standard model species, and $V(\phi, \chi)$ is the interaction potential defined analogously to hybrid inflation,

$$V(\phi, \chi) = \frac{\lambda}{4} (M^2 - \chi^2)^2 + \frac{1}{2} g^2 \phi^2 \chi^2 + \frac{1}{2} \mu^2 \phi^2 \equiv V_0 - \frac{1}{2} \lambda M^2 \chi^2 + \frac{1}{4} \lambda \chi^4 + \frac{1}{2} g^2 \phi^2 \chi^2 + \frac{1}{2} \mu^2 \phi^2. \quad (2)$$

Here, the two scalar fields ϕ and χ assume the roles of DE and DM, respectively, comprising a *hybrid model for the dark sector*. This model exhibits a rich phenomenology, described in detail in [50]. In this work, we focus on the parameter space leading to an oscillating DM field and a slow-rolling DE field. Consequently, we adopt the following simplified interaction potential,

$$V(\phi, \chi) = V_0 + \frac{1}{2} g^2 \phi^2 \chi^2, \quad (3)$$

where we assume that the last term in Eq. (2) is smaller than the interaction term. The requirement for χ to oscillate in the effective potential is expressed as $m_\chi^2 > H^2$, while for ϕ to evolve slowly as DE, $m_\phi^2 < H^2$, where the effective masses are given by

$$m_\chi^2 = g^2 \phi^2, \quad (4)$$

$$m_\phi^2 = g^2 \chi^2. \quad (5)$$

We note that, since χ oscillates faster than the Hubble expansion rate, m_ϕ^2 is proportional to the density of the χ field. This results in the source term on the right-hand side in Eq. (9) below.

The conditions on the masses translate into the following constraint on the value of the ϕ field [50]:

$$1 < \frac{1}{3} \left(\frac{\phi}{M_{\text{Pl}}} \right)^2. \quad (6)$$

When the value of the ϕ field becomes small enough to violate this condition, the χ field ceases oscillating, implying that DM will no longer exist in its current form. Both fields then settle at the global minimum of the potential (where $V = 0$), ending the accelerated expansion.

To reduce computational costs, we average the DM field χ over a period of oscillation and solve for the averaged energy density of DM, ρ_c ,

$$\rho_c = \frac{1}{2} \dot{\chi}^2 + \frac{1}{2} g^2 \phi^2 \chi^2, \quad (7)$$

alongside the scalar field DE, ϕ . The procedure is detailed in [50]. The resulting equations of motion in Planck units are,

$$\dot{\rho}_c + 3H\rho_c = \frac{\dot{\phi}}{\phi}\rho_c, \quad (8)$$

$$\ddot{\phi} + 3H\dot{\phi} = -\frac{1}{\phi}\rho_c. \quad (9)$$

The coupling between DM and DE is proportional to $1/\phi$. As shown in [50], the DE scalar field is invariably driven toward the minimum of the potential at very early stages when its contribution is effectively negligible for the cosmological evolution. For this reason, the initial velocity of the DE scalar field $\dot{\phi}_i$ does not have a relevant impact on the dynamics, and so, without loss of generality, we always set $\dot{\phi}_i = 0$. Hence, the system's modified dynamics are fully determined by the initial value of the DE field, ϕ_i . This model is thus a one-parameter extension of the Λ CDM model.¹ For the data analysis in the following sections, we sample the initial value of the coupling parameter $1/\phi_i$, which is more intuitive and defines a compact parameter range. In the limit $1/\phi_i \rightarrow 0$, Λ CDM is recovered. Larger coupling values [corresponding to ϕ_i closer to the theoretical limit in Eq. (6)] lead to greater deviations from standard cosmology.

We demonstrate the main effect of the coupling in Fig. 1, showing deviations from Λ CDM by introducing the following reparametrization of the background DE density [60,61],

$$\rho_{\phi,\text{eff}}(a) = \rho_\phi + \rho_c(a) - \rho_{c,0}a^{-3}. \quad (10)$$

The quantity $\rho_{\phi,\text{eff}}$ describes an effective dark energy fluid, which includes the DE component plus the non-standard component of DM arising due to the interaction in the dark sector, effectively mimicking an uncoupled dark sector at the level of the background. In other words, it encloses the deviation from the standard Λ CDM evolution in a single component. The evolution of $\rho_{\phi,\text{eff}}$ is given by

$$\dot{\rho}_{\phi,\text{eff}} + 3H\rho_{\phi,\text{eff}}(1 + w_{\phi,\text{eff}}) = 0, \quad (11)$$

where we have defined the effective equation of state

$$w_{\phi,\text{eff}} = \frac{P_\phi}{\rho_{\phi,\text{eff}}}. \quad (12)$$

This effective equation of state is the equation of state of DE, *assuming* an uncoupled DM species, as it is usually taken as given when analysing low-redshift data such as supernovae. In Fig. 1, we show the equation of state (EoS) parameter of this effective dark energy sector, supposing standard CDM evolution.

¹In this framework, V_0 is merely the scale of the potential, not a true degree of freedom, that is used to numerically enforce the closure relation $\sum_i \Omega_i = 1$ through a shooting method.

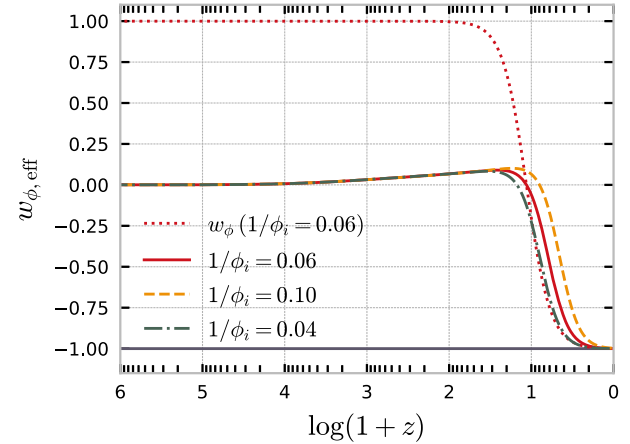


FIG. 1. Effective DE equation of state parameter defined in Eq. (12) for different values of ϕ_i . All cosmological parameters are fixed to the mean values for the hybrid model under the Pl18 + DESI data combination for various values of the coupling parameter $1/\phi_i$: the mean value obtained from the data analysis is shown in red, $1/\phi_i = 0.1$ is shown in dashed yellow, and $1/\phi_i = 0.04$ is shown in dotted-dashed green. In dotted red, we depict the equation of state parameter for the DE scalar field alone w_ϕ (i.e., excluding the effective DM contribution) for the Pl18 + DESI scenario for reference. While in the matter-dominated epoch, the effective EoS parameter is dominated by the CDM-like contribution from the coupling in the dark sector, at late times, it is driven down by the w_ϕ contribution.

The effective DE behavior can be dissected from the individual evolutions of ρ_c and ρ_ϕ : As described in [50], the ρ_ϕ component tracks the DM during the matter domination era until its kinetic part decays enough for the constant potential to take over, at which point it transitions to a cosmological constant. The ρ_c component starts as standard CDM at early times, then diluting faster than a^{-3} when the ϕ field starts to evolve, and the coupling turns on. As a result, the effective DE field behaves as an additional DM component at early times until matter domination. At this point, the effective EoS becomes positive and $\rho_{\phi,\text{eff}}$ is dominated by the ρ_c contribution. At late times, the EoS transitions back to that of a cosmological constant. This means that, effectively, a fraction of the DM energy density becomes DE at late times. Although it resembles tracking dark energy (e.g., [62]), it is also different from such models as the DE field does not always scale with the dominant component in this effective description.

It is also important to note that the coupling constant g present in the potential in Eq. (3) is absent from the effective fluid equations (see [50] for more details), meaning that its value cannot be constrained under this fluid approximation. This, in turn, implies that the masses of DM and DE are not constrained in this model, as they depend linearly on g . Nevertheless, g controls the validity of the time-averaged description of χ directly through the mass of both scalars ($m_\chi = g\phi$ and $m_\phi = g|\chi|$). In practice we

require $m_\chi \gg H$ (fast χ oscillations) and $m_\phi \ll H$ (slow-rolling ϕ). For values of g so small such that $g\phi \lesssim H$ during the relevant epochs the averaging would fail and the fluid approximation would no longer hold. Conversely, in Sec. III B, we will use our best-fit results to derive an upper limit on g .

The dynamics of the hybrid model also introduce modifications at the level of the linear perturbations in comparison to Λ CDM. We refer to [50] for the complete derivation of the perturbation equations and a discussion of the evolution of cosmological perturbations in this model. This work aims to constrain the hybrid model with cosmological data, which is the focus of the remainder of the paper.

III. ANALYSIS

A. Methodology and datasets

We implement the relevant equations for the hybrid model in our modified version of the Einstein-Boltzmann solver code `CLASS`² [63–65]. We perform a Markov chain Monte Carlo (MCMC) analysis by interfacing the solver with the publicly available sampler `Monte Python`³ [66,67] to confront the hybrid model with recent cosmological data. Cosmological and nuisance parameters are varied according to Cholesky’s parameter decomposition [68]. We consider chains to be converged with the Gelman-Rubin convergence criterion $R - 1 < 10^{-2}$ [69]. The corresponding chains are treated and analysed using the `GetDist`⁴ Python package [70].

We assume wide uniform priors for the set of sampled cosmological parameters $\{\Omega_b h^2, \Omega_c h^2, 100\theta_s, \tau_{\text{reio}}, n_s, \log(10^{10}A_s)\}$ in the range detailed in Table I. These are the standard Λ CDM parameters, namely the physical density of baryonic matter today, the physical density of dark matter today, the angular scale of the sound horizon at the time of last scattering, the optical depth to reionization, the scalar spectral index, and the amplitude of the primordial scalar power spectrum at the pivot scale $k_{\text{pivot}} = 0.05 \text{ Mpc}^{-1}$. Regarding the free parameter of the hybrid model, the initial condition of the dark energy scalar field ϕ_i , we opt for sampling over its inverse $1/\phi_i$ to reduce the impact of the diverging parameter space in which the model reduces to the Λ CDM limit ($\phi_i \gg 1$), with a uniform prior covering the range of validity of the model’s assumptions. The other independent parameters are fixed to their *Planck* best-fit values [30], including the assumption of two massless and one massive neutrino species with $m_\nu = 0.06 \text{ eV}$. Although not explicitly listed, a large number of nuisance parameters are varied simultaneously, following the respective collaboration recommendations.

TABLE I. Flat priors on the cosmological and model parameters sampled in this work.

Parameter	Prior
$\Omega_b h^2$	[0.005, 0.1]
$\Omega_c h^2$	[0.001, 0.99]
$100\theta_s$	[0.5, 10]
τ_{reio}	[0.02, 0.08]
n_s	[0.7, 1.3]
$\log(10^{10}A_s)$	[1.7, 5.0]
$1/\phi_i$	[0, 1]

The datasets considered are the ones listed below:

- (i) *Planck* 2018 (Pl18): The *Planck*-2018 CMB high- ℓ TTTEEE, low- ℓ TTEE, and lensing likelihoods [30,71,72]. Specifically, this includes the high- ℓ *Plik* likelihood for TT over the range $30 \leq \ell \leq 2508$, and for TE and EE within $30 \leq \ell \leq 1996$, combined with the low- ℓ TT and EE likelihoods for $2 \leq \ell \leq 29$, based on the *Commander* algorithm and the *SimAll* likelihood. Although newer versions of the *Planck* likelihood have been developed [73,74], we use the baseline collaboration likelihood and expect only slightly tighter constraints with alternative likelihoods, which will not impact our main results.
- (ii) *DESI*: The baryonic acoustic oscillations (BAO) measurements obtained from the first year of Dark Energy Spectroscopic Instrument (DESI) observations. These data are based on galaxy and quasar observations [75] as well as Lyman- α tracers [76], as detailed in Table I of Ref. [51]. Covering an effective redshift range of approximately $z \sim 0.1\text{--}4.1$, the measurements include the transverse comoving distance (D_M/r_d), the Hubble horizon (D_H/r_d), and the angle-averaged distance (D_V/r_d), each normalized to the comoving sound horizon at the drag epoch, r_d . The appropriate correlations between measurements of D_M/r_d and D_H/r_d are considered in the computations.
- (iii) *Pantheon*-plus (supernovae (SN)): The *Pantheon* + catalog distance modulus measurements derived from 1701 light curves of 1550 Type Ia supernovae (SNeIa), detected spectroscopically, spanning a redshift range of $0.001 < z < 2.26$. The data, compiled in the *Pantheon*-plus sample [77,78], include observed magnitudes postprocessed for systematic effects, with residual corrections and marginalization over nuisance parameters [79]. These can be translated into uncalibrated luminosity distances of the SNeIa.
- (iv) *Pantheon*-plus with SH_0 ES R22 (SH0ES): In our analysis, we consider the *Pantheon*-plus sample with and without the SH_0 ES Cepheid host distance anchors as calibrators [11], typically employed to address degeneracies in the $M - H_0$ plane.

²https://github.com/lesgourg/class_public

³https://github.com/brinckmann/montepython_public

⁴<https://github.com/cmbant/getdist>

Our baseline dataset is Planck 2018, denoted as “Pl18,” to which we incrementally add other combinations to assess the constraints imposed by each dataset on the model. Separate combinations with DESI BAO and Pantheon-plus data are referred to as “Pl18 + DESI” and “Pl18 + DESI,” respectively, while the full addition of background data to the CMB is denoted as “Pl18 + DESI + SN.” Finally, whenever the SH₀ES Cepheid anchors are considered, the “SN” data is represented as “SH0ES,” and the inclusion of all datasets is denoted as “Pl18 + DESI + SH0ES.”

B. Results

In this section, we discuss the constraints placed by each dataset combination on the hybrid model in direct comparison with the Λ CDM model. Table II summarizes the

results of the analysis described in Sec. III A for the {Pl18, Pl18 + DESI, Pl18 + SH0ES, Pl18 + DESI, Pl18 + DESI + SN, Pl18 + DESI + SH0ES} datasets at the 68% confidence level (CL). The corresponding 1D and 2D marginalized posterior distributions are depicted in Figs. 2 and 3 for relevant parameters and key data combinations at 68% and 95% CL. Similar tables for the same datasets in the Λ CDM model can be found in Appendix A, along with additional contour plots and the same analysis with a different BAO sample.

To determine the model preference in terms of the fit to each data combination, we report the difference in the value of the minimum χ^2 with respect to the Λ CDM model, $\Delta\chi^2_{\min} = \chi^2_{\min, \text{Hybrid}} - \chi^2_{\min, \Lambda\text{CDM}}$, computed through a global minimization approach using the simulated-annealing

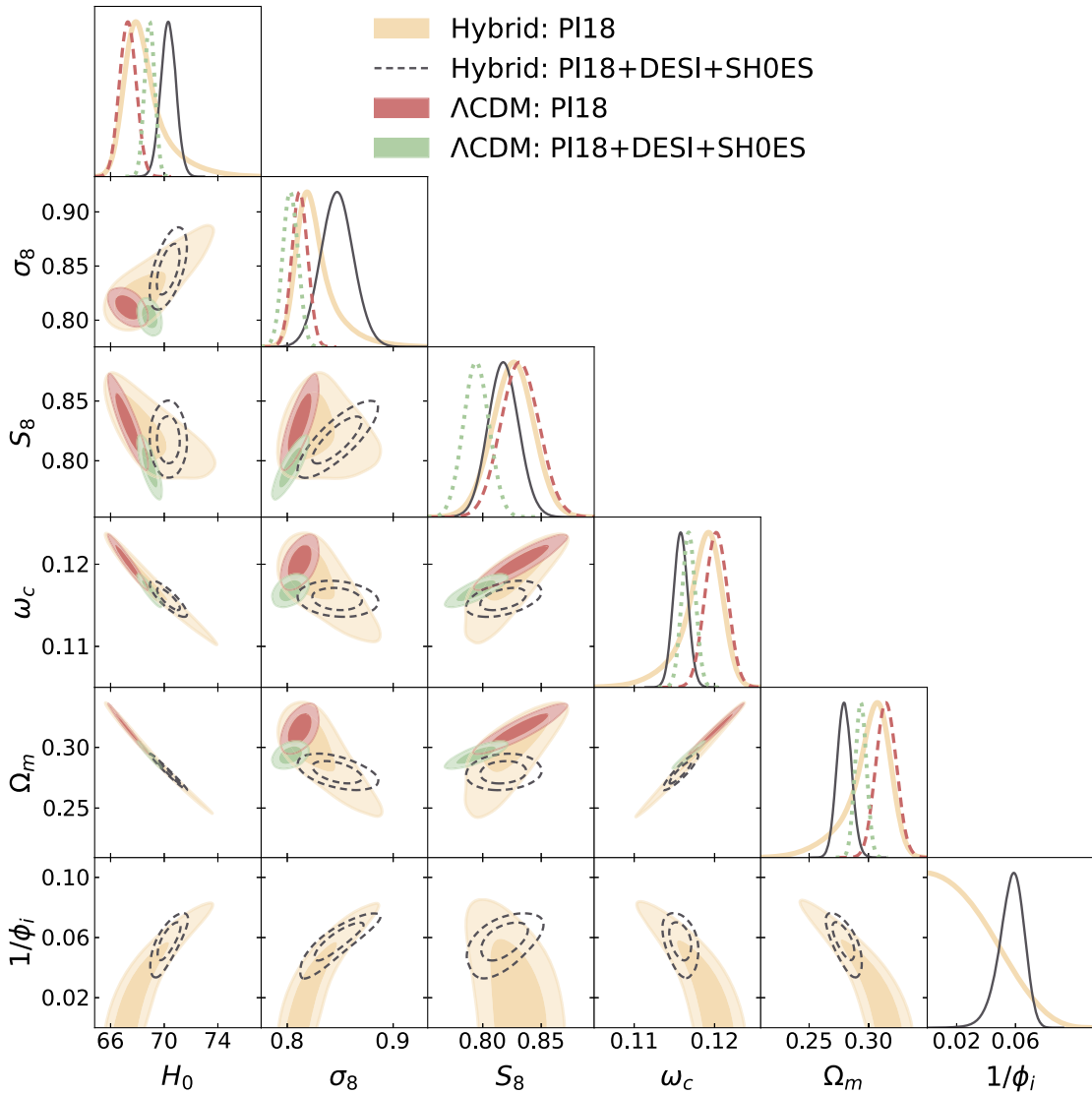


FIG. 2. One-dimensional posterior probability distribution functions and two-dimensional contours at 68% and 95% CL for the parameters of interest in the hybrid model and the standard Λ CDM model for reference, for the minimal Pl18 dataset and the full combination Pl18 + DESI + SH0ES, as indicated in the legend and listed in Sec. III A.

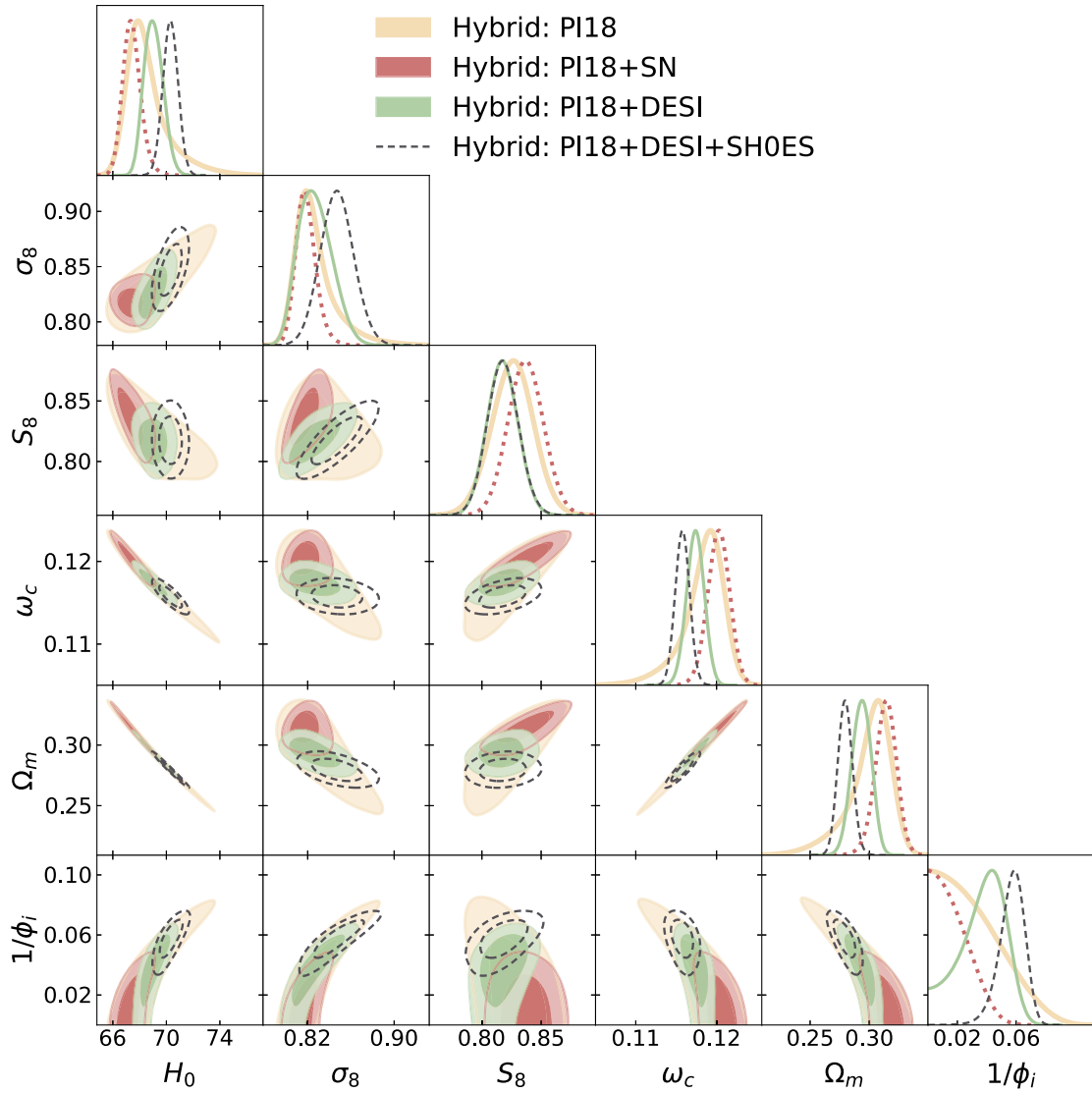


FIG. 3. One-dimensional posterior probability distribution functions and two-dimensional contours at 68% and 95% CL for the parameters of interest in the hybrid model for incremental dataset combinations, as indicated in the legend and listed in Sec. III A.

optimizer Procol⁵ package [80]. A negative value of $\Delta\chi^2_{\min}$ indicates a better fit for the hybrid model, while a positive value suggests otherwise. Additionally, we report on the Bayesian evidence $\log B_{M,\Lambda\text{CDM}}$ test for model comparison, for which we employed the public MCEvidence⁶ code [81,82]. The greater the evidence for the hybrid model relative to ΛCDM , the larger the Bayes factor ratio (the difference of the logarithms) will be. Furthermore, if its value is negative, there is no evidence supporting the hybrid model over ΛCDM for a given dataset, while the opposite holds if it is positive.

Finally, the difference of the maximum *a posteriori* (DMAP) metric tension for H_0 given a particular dataset D is [83]

$$Q_{\text{DMAP},D}^{\text{SH0ES}} = \sqrt{\chi^2_{\min}(D + M_B) - \chi^2_{\min}(D)}, \quad (13)$$

which is used to assess the compatibility between the constraints derived for the model under the dataset D and the $SH_0\text{ES}$ prior on the value of H_0 .⁷ This method has the added benefit of being insensitive to prior volume effects,

⁷The formulation of the DMAP metric tension in Eq. (13) is only valid for datasets differing by one degree of freedom. Since when imposing the $SH_0\text{ES}$ calibration as listed in Sec. III A we consider only a subsample of the supernovae in the entire Pantheon-plus catalog, we opt instead for replacing the full $SH_0\text{ES}$ likelihood with the Pantheon-plus sample plus a Gaussian prior on the absolute magnitude calibration M_B of the supernovae in $SH_0\text{ES}$ [11]. We use this approximation for the sole purpose of computing $Q_{\text{DMAP},D}^{\text{SH0ES}}$, and we have confirmed that it does not impact the results.

⁵<https://github.com/tkarwal/procol>

⁶<https://github.com/yabebalFantaye/MCEvidence>

TABLE II. Observational constraints at a 68% confidence level on the independent and derived cosmological parameters using different dataset combinations for the hybrid model, as detailed in Sec. III A. $\Delta\chi^2_{\min}$ represents the difference in the best-fit χ^2 of the profile likelihood global minimization, and $\log B_{M,\Lambda\text{CDM}}$ indicates the ratio of the Bayesian evidence, both computed with respect to ΛCDM . The value of $Q_{\text{DMAP}}^{\text{SHOES}}$ is calculated according to Eq. (13). For reference, the same results for ΛCDM are given in Table III of Appendix A.

Parameter	Pl18	Pl18 + SN	Pl18 + SH0ES	Pl18 + DESI	Pl18 + DESI + SN	Pl18 + DESI + SH0ES
ω_b	0.02236 ± 0.00015	0.02231 ± 0.00014	0.02237 ± 0.00015	0.02240 ± 0.00015	0.02239 ± 0.00015	0.02237 ± 0.00015
ω_c	$0.1184^{+0.0029}_{-0.0016}$	0.1202 ± 0.0014	0.1139 ± 0.0014	0.1174 ± 0.0011	0.11820 ± 0.00099	0.11577 ± 0.00089
$100\theta_s$	1.04187 ± 0.00030	1.04182 ± 0.00029	1.04190 ± 0.00030	1.04193 ± 0.00030	1.04194 ± 0.00029	1.04188 ± 0.00029
τ_{reio}	0.0548 ± 0.0077	0.0539 ± 0.0077	0.0558 ± 0.0079	0.0557 ± 0.0079	0.0557 ± 0.0077	0.0554 ± 0.0078
n_s	0.9660 ± 0.0045	0.9640 ± 0.0041	0.9683 ± 0.0041	0.9677 ± 0.0040	0.9673 ± 0.0039	0.9670 ± 0.0041
$\log 10^{10} A_s$	3.047 ± 0.016	3.046 ± 0.016	3.049 ± 0.016	3.047 ± 0.016	3.047 ± 0.016	3.048 ± 0.016
$1/\phi_i$	< 0.0390	< 0.0220	$0.0661^{+0.0095}_{-0.0073}$	$0.037^{+0.019}_{-0.012}$	$0.029^{+0.017}_{-0.015}$	$0.0570^{+0.0096}_{-0.0070}$
Best fit:	[0.0054]	[0.0019]	[0.0676]	[0.0455]	[0.0341]	[0.0591]
σ_8	$0.8263^{+0.0095}_{-0.021}$	$0.8185^{+0.0079}_{-0.010}$	0.858 ± 0.017	$0.827^{+0.013}_{-0.018}$	$0.821^{+0.010}_{-0.015}$	0.847 ± 0.015
H_0	$68.55^{+0.80}_{-1.8}$	$67.42^{+0.59}_{-0.72}$	71.49 ± 0.87	$69.04^{+0.65}_{-0.76}$	$68.51^{+0.51}_{-0.63}$	70.30 ± 0.56
Ω_m	$0.300^{+0.021}_{-0.011}$	$0.3138^{+0.0093}_{-0.0084}$	0.2669 ± 0.0091	0.2934 ± 0.0080	$0.2997^{+0.0073}_{-0.0065}$	0.2796 ± 0.0061
S_8	0.826 ± 0.018	0.837 ± 0.015	0.809 ± 0.014	0.817 ± 0.013	0.821 ± 0.013	0.818 ± 0.013
$\Delta\chi^2_{\min}$	0.14	0.08	-16.32	-2.8	-1.06	-12.76
$\log B_{M,\Lambda\text{CDM}}$	-3.3	-3.6	4.5	-2.0	-2.8	2.5
$Q_{\text{DMAP}}^{\text{SHOES}}$...	4.78	4.65	...

and the global maximum likelihood values are derived directly from Procoli.

At the end of Table II, we list the $\Delta\chi^2_{\min}$ values and the associated Bayesian evidence compared to ΛCDM for all the data combinations, and also the $Q_{\text{DMAP},\text{D}}^{\text{SHOES}}$ tension for the relevant cases. In Table VI of Appendix C, we list in detail the χ^2_{\min} values associated with each likelihood for the different models and data combinations used in this study.

We summarize our main findings below, based on the results in the above figures and tables.

Considering only the baseline CMB Pl18 data, the hybrid model provides a similar fit to ΛCDM , with a negligible $\Delta\chi^2_{\min}$ and no detection of the coupling parameter at 1σ : $1/\phi_i < 0.039$. In Fig. 2, we see that the constraints derived for the hybrid model (beige) are very similar to the ΛCDM case (red), but with enlarged errors due to the long tail in the $1/\phi_i$ 1D posterior. Moreover, the increased prior volume implies that the hybrid model is disfavored with respect to ΛCDM regarding the Bayesian evidence. Nevertheless, the positive correlation between $1/\phi_i$ and H_0 and negative correlation with S_8 allows us to relax the constraint to H_0 and S_8 from Pl18 data alone, suggesting a potential role in cosmic tensions.

As expected, including the BAO data from DESI significantly improves the constraining power by breaking the geometrical degeneracies in the CMB, making the data more sensitive to the particular effects of the dynamical behavior of the dark sector at late times in the hybrid model. More precisely, for the Pl18 + DESI combination, we find

a detection of the coupling at 2σ with $1/\phi_i = 0.037^{+0.019}_{-0.012}$ and $1/\phi_i = 0.037^{+0.025}_{-0.033}$ at 68% and 95% CL, respectively. This data combination is represented in green in Fig. 3, where we see that not only do the contours generally shrink in relation to Pl18 (beige), but also the 1D marginalized posterior distribution for $1/\phi_i$ shows a well-defined peak away from the standard cosmological model limit $1/\phi_i \rightarrow 0$. This contrasts with what is found for the Sloan Digital Sky Survey (SDSS) BAO dataset (see Fig. 8 in Appendix A), where the BAO data reinforces the general preference for a cosmology consistent with a cosmological constant [84]. Including DESI data brings $\Delta\chi^2_{\min}$ down by -2.8, indicating a better fit in the hybrid model. The Bayesian evidence remains negative, showing no preference for the hybrid model.

The inclusion of the SN distance moduli measurements alone yields similar results to the Pl18-alone case, with only mild reductions in the error bars of the cosmological parameters, actually bringing $1/\phi_i$ closer to zero: $1/\phi_i < 0.0220$. The addition of the SH0ES calibration (Pl18 + SN + H_0) inevitably pushes H_0 toward higher values, resulting in an apparent detection of the coupling at more than 3σ : $1/\phi_i = 0.066^{+0.019}_{-0.028}$ at 99% CL.

The full combination of “background” data (Pl18 + DESI + SN) leads to constraints that are essentially unchanged relative to the Pl18 + DESI case but with a detection of $1/\phi_i$ only at 1σ given the preference for consistency with ΛCDM found for the SN data: $1/\phi_i = 0.029^{+0.017}_{-0.015}$ at 68% CL. Analogously, the inclusion of the

SH_0 ES calibration for the SN (Pl18 + DESI + SH0ES) results in a larger predicted value for H_0 , and detection of the coupling in the hybrid model at more than 3σ : $1/\phi_i = 0.057^{+0.019}_{-0.029}$ at 99% CL.

Once the SH_0 ES calibration is included, we observe an increase in $\Delta\chi^2_{\text{min}}$, going from 0.08 to -16.32 in the Pl18 + SH0ES case and from -1.06 to -12.76 in Pl18 + SH0ES. The Bayesian evidence also indicates moderate to strong support for the hybrid model, according to the Jeffreys scale [85]. However, the Q_{DMAP} indicator shows that there is still a large residual tension between the datasets. The breakdown of χ^2_{min} in Table VI shows that the tension is indeed hidden in a worsened fit to the Pl18 and DESI likelihoods compared to the case without the calibration. With respect to Λ CDM, there is a better fit to Pl18 and SH0ES in the hybrid case but a worse fit to DESI.

Overall, the hybrid model leads to a slight alleviation of the H_0 tension, with $Q_{\text{DMAP,Pl18+SN}}^{\text{SH0ES}} = 4.78\sigma$ and $Q_{\text{DMAP,Pl18+DESI+SN}}^{\text{SH0ES}} = 4.65\sigma$, compared to $Q_{\text{DMAP,Pl18+SN}}^{\text{SH0ES}} = 6.25\sigma$ and $Q_{\text{DMAP,Pl18+DESI+SN}}^{\text{SH0ES}} = 5.76\sigma$ for Λ CDM. This expresses only a mild reduction of the H_0 tension in the hybrid model. The H_0 tension is of the same order regardless of the inclusion of DESI in the baseline dataset since the posteriors obtained are compatible at 1σ , and the value of H_0 needed to fit the cosmology in this case is still too low. As expected, once the SH_0 ES SN calibration is added to the analysis, the predicted value of $H_0 \sim 70$ is a compromise between the two incompatible values, reflecting the tension in the datasets

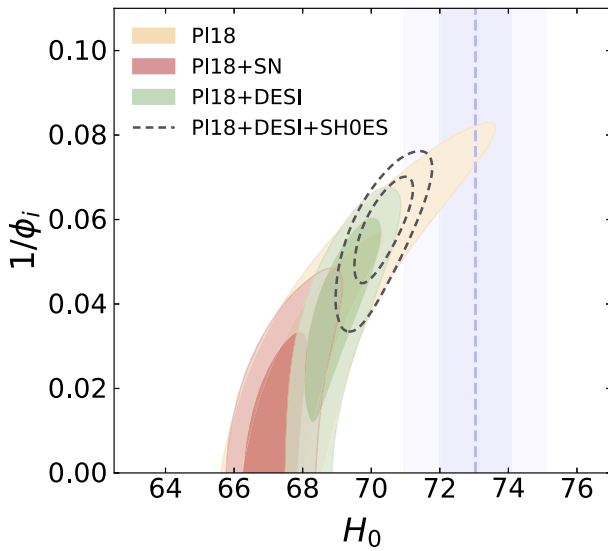


FIG. 4. 2D contours at 68% and 95% CL for the initial condition of the scalar field $1/\phi_i$ and the Hubble parameter H_0 (in units of km/s/Mpc). The results are inferred considering different combinations of *Planck* 2018, DESI BAO distance, and SN distance moduli data, as indicated in the legend and listed in Sec. III A. The blue dashed line and band represent the value of H_0 measured by the SH_0 ES collaboration and the respective uncertainties.

under the model in consideration. This effect is illustrated in Fig. 4, where we display the 2D contours for the model parameter $1/\phi_i$ and H_0 for the incremental datasets used in this analysis.

The origin of the correlation between $1/\phi_i$ and H_0 can be traced back to the ω_c panels of Fig. 3: Therein, we observe that there is a negative correlation between ω_c and $1/\phi_i$ for all the datasets considered, implying that stronger interactions lead to a preference toward lower values of ω_c . Physically, increasing $1/\phi_i$ enhances the early-time DM-like contribution of $\rho_{\phi,\text{eff}}$, effectively advancing matter–radiation equality and boosting early growth. This smaller ω_c allows one to compensate the larger h , yielding an overall smaller Ω_m , which helps in keeping the angular diameter distance to recombination (and therefore the angular size of the sound horizon) fixed. Note that this mechanism is different from regular dynamical dark energy, which requires a phantom behavior (e.g., [86]). In Fig. 5, we illustrate the impact of the interaction on the evolution of the dark matter energy density for the hybrid model. We fix the cosmological parameters (and hence the value of ω_c) to the best-fit value found for the hybrid model with the full combination of Pl18 + DESI + SH0ES. Under Λ CDM (yellow line), this results in a consistent overall shift in the ratio of dark matter relative to the Λ CDM best-fit (grey line). In the case of the hybrid model (red dashed line), this ratio evolves with redshift according to the impact of the interaction, which can be understood as an additional redshift-dependent contribution to ρ_c coming from the effective fluid described in Eq. (12). As a result, ρ_c is slightly larger than in (standard) Λ CDM originally and

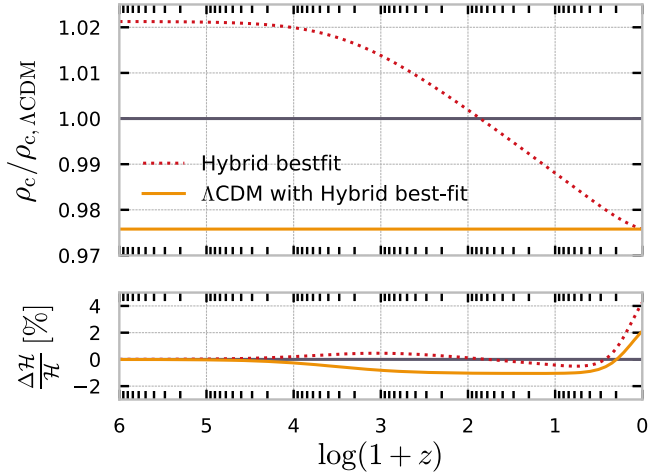


FIG. 5. *Top panel*: redshift evolution of the dark matter energy density for the hybrid model (dotted red) and Λ CDM model (filled yellow), with cosmological parameters fixed to the best fit of the hybrid model under the Pl18 + DESI + SH0ES dataset combination in both cases. The corresponding case of the Λ CDM best fit is depicted in grey for reference. *Bottom panel*: percent relative deviations in the value of the Hubble rate with respect to the Λ CDM Pl18 + DESI + SN best fit for the same scenarios.

decays to about 97.5% of its value at late times. Note also that the larger effective DM density at early times, which enhances the linear growth prior to the late-time transfer of energy from DM to DE, implies that σ_8 increases in the hybrid model. However, the weak-lensing parameter S_8 receives an overall suppression due to the smaller Ω_m .

From the results obtained from the combination of *Planck* 2018 and DESI BAO distance measurements, there is some evidence to support the interaction between DE and DM through the hybrid fluid approximation. Indeed, it is known that DESI data attempts to bring the physical matter density down in Λ CDM. At face value, this leads to a slight disagreement between DESI and Pl18 ($\sim 2\sigma$) under Λ CDM. As a result, the time-dependence of ρ_c in the hybrid model is favored when DESI is added to the baseline dataset, with $\Delta\chi^2_{\min} = 0.14$ in Pl18 going to $\Delta\chi^2_{\min} = -2.8$ for Pl18 + DESI. However, this is not supported by Pantheon-plus data, which favors a larger Ω_m than DESI. In the analysis reported by the DESI collaboration [51] for minimal parametrizations of dynamical dark energy, a considerable preference in favor of phantom dark energy over Λ CDM (with the combination of *Planck* 2018, DESI, and SNIa data) was reported and has been the focus of multiple studies. In the context of the hybrid model, the preference for a late-time effective phantomlike behavior for DE is replaced by the coupled dark sector with a nonvanishing detection of $1/\phi_i > 0$ exceeding the 95% CL. The phenomenological difference in the dynamics of DE under the hybrid model compared to the CPL [87,88] parametrization highlighted in the DESI Y1 data release [51] is illustrated in Fig. 6 with $w_{\phi,\text{eff}}$ as defined in Eq. (12), mimicking DE in an uncoupled dark sector. We stress that in that case, $w_{\phi,\text{eff}}$ never becomes phantom. This suggests

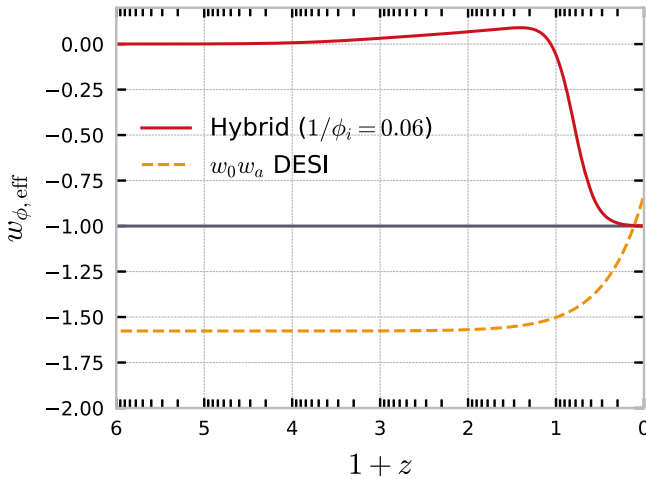


FIG. 6. Redshift evolution of the effective EoS parameter of DE in the hybrid model with the Pl18 + DESI + SH0ES best fit (in filled red) compared with the EoS parameter for DE reported by the DESI collaboration (in dashed yellow) for a CPL w_0w_a parametrization under Pl18 + DESI + SN with best-fit values $w_0 = -0.827$ and $w_a = -0.75$ [51].

an alternative explanation to the mild discrepancy between DESI and Pl18. However, this behavior does not help reconcile Pl18 + DESI data with the (uncalibrated) SNe, which favor larger Ω_m and a phantom DE behavior [89,90]. Future BAO and SNe data are thus crucial for the fate of the hybrid model.

Finally, using Eq. (4) in conjunction with our best-fit results, we can put an upper limit on the coupling constant g . For Planck+DESI+SH0ES, we find the best-fit value $\phi_i = 16.92 M_{\text{Pl}}$. Requiring that the DM mass is smaller than the Planck mass yields the most conservative upper limit on the value of g . However, another conservative requirement is ensuring that the DM is not oscillating during inflation: requiring $m_\chi \lesssim 10^{12}$ GeV leads to $g \lesssim 10^{-8}$. Stronger upper limits on the DM mass will put more stringent constraints on the value of the coupling constant g .

IV. CONCLUSIONS

In this work, we have explored the predictions of the hybrid model proposed in [50] and its fit to currently available datasets, namely *Planck* 2018 CMB data, the Pantheon + catalog of SN distance moduli—with and without the Cepheid calibration from SH0ES—and the recent BAO distance measurements by the DESI collaboration. From the phenomenological side, this model has interesting features derived from a Lagrangian formulation with a fluid description motivated by the physics of the dark sector. The model extends the standard Λ CDM framework by introducing one single additional parameter, the initial value of the DE scalar field ϕ (ϕ_i), which governs the strength of the interaction between dark matter and dark energy ($\propto 1/\phi_i$). On the observational side, the main effect of this coupling is to provide a nontrivial time dependence to the dark matter and dark energy densities as the effective DE field transitions from behaving like DM at early times to regular DE at late times. As a result, the dynamics of the scalar field and the dark sector interaction induce a negative correlation between the physical density of dark matter ω_c and the coupling parameter. This correlation helps accommodate the tendency of the DESI data to bring the matter density down in Λ CDM, leading to a better fit to this dataset in the hybrid model. At the same time, this is also entangled with a positive correlation between $1/\phi_i$ and H_0 (required to preserve the angular diameter distance to recombination), making it possible to alleviate the Hubble tension slightly.

Our main conclusions regarding the hybrid model in light of CMB, BAO and SNe data are as follows:

- (i) For Pl18 alone, the hybrid model is virtually indistinguishable from Λ CDM in terms of the quality of the fit ($\Delta\chi^2_{\min} \simeq 0$), and we derive an upper bound on the initial field value $1/\phi_i < 0.0390$.
- (ii) When DESI data are included, the hybrid model provides a better fit than Λ CDM, thanks to the ability to accommodate the lower Ω_m favored by

DESI. The inclusion of (uncalibrated) Pantheon-plus data, however, reduces the relative improvement in χ^2 , and the Bayesian evidence comparison remains inconclusive for most combinations, often favoring ΛCDM due to the increased prior volume.

- (iii) The hybrid model demonstrates potential to slightly alleviate the Hubble tension, with a relaxation of the constrain to H_0 , allowing for values closer to those from $SH_0\text{ES}$ measurements when combining all datasets. However, the alleviation is insufficient to eliminate the tensions, estimated to be 4.65σ in the hybrid model down from 5.76σ in ΛCDM .
- (iv) The coupling parameter $1/\phi_i$ correlates positively with σ_8 due to the additional DM contribution at early times, but the decrease in Ω_m at late times dominates, yielding a slightly smaller S_8 .

Overall, while the hybrid model offers promising avenues for addressing theoretical questions related to the nature of the dark sector and observational issues such as the cosmological tensions, whether it provides a better fit to available data in comparison with ΛCDM is dataset dependent, and significant challenges remain in reconciling all the observational incompatibilities within this framework. Nevertheless, the ability to introduce time dependence in the DM (and DE) densities is an interesting phenomenological feature of the model, which helps address DESI measurements and accommodate larger H_0 values. In this study, we focused on purely adiabatic initial conditions. The impact of isocurvature modes on the constraints is worth investigating in future work.

In light of these results, we highlight the importance of phenomenological models of the dark sector, which, through their inherent dynamics, can address the cosmological tensions under specific regimes. We emphasize the need to investigate the phenomenological predictions of such models when faced with the available observational data.

The authors acknowledge the use of high-performance computing resources from the IT Services at the University

of Sheffield and the CNRS IN2P3 Computing Centre (CC-IN2P3).

ACKNOWLEDGMENTS

We thank Thomas Montandon and William Giarè for numerical support and valuable discussions. V. P. and E. M. T. are supported by funding from the European Research Council (ERC) under the European Union's HORIZON-ERC-2022 (Grant Agreement No. 101076865). E. M. T. was also supported by the Grant No. SFRH/BD/143231/2019 from Fundação para a Ciência e a Tecnologia (FCT) during the initial stages of this work. G. P. is supported by an EPSRC studentship. C. vdB. is supported by the Lancaster-Sheffield Consortium for Fundamental Physics under STFC Grant No. ST/X000621/1. E. D. V. is supported by a Royal Society Dorothy Hodgkin Research Fellowship. This article is based upon work from COST Action CA21136 Addressing observational tensions in cosmology with systematics and fundamental physics (CosmoVerse) supported by COST (European Cooperation in Science and Technology).

DATA AVAILABILITY

The data analyzed in this paper are openly available, with references given in Sec. III in our article. The statistical data that support our findings are not publicly available upon publication because it is not technically feasible and/or the cost of preparing, depositing, and hosting the data would be prohibitive within the terms of this research project.

APPENDIX A: RESULTS FOR ΛCDM AND ALTERNATIVE DATA

In this appendix, we provide results for additional dataset combinations considered in the analysis, along with the ΛCDM counterparts. Table III follows the same organization as Table II, with the results pertaining to the ΛCDM model

TABLE III. Observational constraints at a 68% confidence level on the independent and derived cosmological parameters using different dataset combinations for the ΛCDM model, as detailed in Sec. III A. The value of $Q_{\text{DMAP}}^{\text{SHOES}}$ is calculated according to Eq. (13).

Parameter	Pl18	Pl18 + SN	Pl18 + SHOES	Pl18 + DESI	Pl18 + DESI + SN	Pl18 + DESI + SHOES
ω_b	0.02235 ± 0.00015	0.02231 ± 0.00015	0.02264 ± 0.00014	0.02249 ± 0.00013	0.02246 ± 0.00013	0.02265 ± 0.00013
ω_c	0.1202 ± 0.0014	0.1207 ± 0.0013	0.1169 ± 0.0011	0.11817 ± 0.00094	0.11862 ± 0.00091	0.11678 ± 0.00083
$100\theta_s$	1.04187 ± 0.00030	1.04182 ± 0.00029	1.04221 ± 0.00028	1.04206 ± 0.00028	1.04203 ± 0.00028	1.04223 ± 0.00028
τ_{reio}	0.0543 ± 0.0078	0.0536 ± 0.0077	0.0591 ± 0.0079	0.0572 ± 0.0078	0.0565 ± 0.0077	0.0595 ± 0.0078
n_s	0.9647 ± 0.0045	0.9635 ± 0.0042	0.9729 ± 0.0039	0.9697 ± 0.0038	0.9686 ± 0.0036	0.9733 ± 0.0035
$\log 10^{10} A_s$	3.045 ± 0.016	3.045 ± 0.016	3.048 ± 0.016	3.046 ± 0.016	3.046 ± 0.016	3.048 ± 0.016
σ_8	0.8118 ± 0.0074	0.8125 ± 0.0074	0.8026 ± 0.0074	0.8066 ± 0.0071	0.8078 ± 0.0071	0.8030 ± 0.0071
H_0	67.29 ± 0.61	67.08 ± 0.56	68.86 ± 0.49	68.21 ± 0.42	68.01 ± 0.40	68.91 ± 0.38
Ω_m	0.3150 ± 0.0085	0.3179 ± 0.0078	0.2944 ± 0.0062	0.3024 ± 0.0055	0.3050 ± 0.0053	0.2936 ± 0.0047
S_8	0.832 ± 0.016	0.836 ± 0.015	0.795 ± 0.013	0.810 ± 0.012	0.815 ± 0.012	0.794 ± 0.011
$Q_{\text{DMAP}}^{\text{SHOES}}$...	6.25	5.76	...

TABLE IV. Observational constraints at a 68% confidence level on the independent and derived cosmological parameters using different dataset combinations for the Λ CDM model, as detailed in Sec. III A and Appendix A, using the SDSS BAO dataset as an alternative to DESI. We also include a variation of the full data set with the parameter A_L free as detailed in the text. The value of $Q_{\text{DMAP}}^{\text{SHOES}}$ is calculated according to Eq. (13).

Parameter	PI18 + SDSS	PI18 + SDSS + SN	PI18 + SDSS + SHOES	PI18(A_L) + DESI + SHOES
ω_b	0.02241 ± 0.00014	0.02264 ± 0.00014	0.02259 ± 0.00013	0.02283 ± 0.00014
ω_c	0.11943 ± 0.00098	0.1169 ± 0.0011	0.11766 ± 0.00084	0.11579 ± 0.00086
$100\theta_s$	1.04194 ± 0.00028	1.04221 ± 0.00028	1.04214 ± 0.00028	1.04229 ± 0.00028
τ_{reio}	0.0555 ± 0.0077	0.0591 ± 0.0079	0.0583 ± 0.0077	$0.0503^{+0.0090}_{-0.0076}$
n_s	0.9666 ± 0.0038	0.9729 ± 0.0039	0.9711 ± 0.0036	0.9771 ± 0.0037
$\log 10^{10} A_s$	3.046 ± 0.016	3.048 ± 0.016	3.048 ± 0.016	$3.026^{+0.019}_{-0.016}$
A_L	1.251 ± 0.062
σ_8	0.8094 ± 0.0071	0.8026 ± 0.0074	0.8050 ± 0.0070	$0.7913^{+0.0081}_{-0.0072}$
H_0	67.65 ± 0.44	68.86 ± 0.49	68.51 ± 0.37	69.46 ± 0.40
Ω_m	0.3100 ± 0.0059	0.3121 ± 0.0057	0.2988 ± 0.0048	0.2874 ± 0.0048
S_8	0.823 ± 0.012	0.827 ± 0.012	0.803 ± 0.011	0.774 ± 0.012
$Q_{\text{DMAP}}^{\text{SHOES}}$...	6.24

for the $\{\text{PI18}, \text{PI18} + \text{DESI}, \text{PI18} + \text{SHOES}, \text{PI18} + \text{DESI}, \text{PI18} + \text{DESI} + \text{SN}, \text{PI18} + \text{DESI} + \text{SHOES}\}$ datasets.

In this appendix, we also present the results for the same analysis conducted in Sec. III, but replacing the DESI BAO data with the SDSS BAO data:

(i) SDSS: The BAO legacy data from the completed SDSS-IV eBOSS survey, summarized in Table 3 of [84]. This includes transverse BAO measurements from BOSS galaxies [91], eBOSS luminous red galaxies [92,93], eBOSS emission-line galaxies

TABLE V. Observational constraints at a 68% confidence level on the independent and derived cosmological parameters using different dataset combinations for the hybrid model, as detailed in Sec. III A and Appendix A, using the SDSS BAO dataset as an alternative to DESI. We also include a variation of the full data set with the parameter A_L free as detailed in the text. The value of $Q_{\text{DMAP}}^{\text{SHOES}}$ is calculated according to Eq. (13).

Parameter	PI18 + SDSS	PI18 + SDSS + SN	PI18 + SDSS + SHOES	PI18(A_L) + DESI + SHOES
ω_b	0.02237 ± 0.00014	0.02236 ± 0.00014	0.02237 ± 0.00015	0.02264 ± 0.00017
ω_c	0.1190 ± 0.0010	0.11956 ± 0.00097	0.11675 ± 0.00093	0.11542 ± 0.00090
$100\theta_s$	1.04189 ± 0.00029	1.04187 ± 0.00029	1.04187 ± 0.00030	1.04206 ± 0.00031
τ_{reio}	0.0550 ± 0.0078	0.0545 ± 0.0078	0.0549 ± 0.0077	$0.0493^{+0.0085}_{-0.0075}$
n_s	0.9660 ± 0.0038	0.9653 ± 0.0037	0.9662 ± 0.0041	0.9726 ± 0.0044
$\log 10^{10} A_s$	3.047 ± 0.016	3.046 ± 0.016	3.048 ± 0.016	3.031 ± 0.018
A_L	1.201 ± 0.067
$1/\phi_i$	$0.023^{+0.013}_{-0.016}$	$0.020^{+0.010}_{-0.015}$	$0.0517^{+0.0097}_{-0.0074}$	$0.0427^{+0.016}_{-0.0094}$
Best-fit:	[0.0241]	[0.0068]	[0.0538]	[0.0469]
σ_8	$0.8194^{+0.0087}_{-0.013}$	$0.8180^{+0.0084}_{-0.011}$	0.842 ± 0.015	$0.819^{+0.016}_{-0.018}$
H_0	$68.05^{+0.49}_{-0.63}$	$67.76^{+0.45}_{-0.54}$	69.71 ± 0.55	70.18 ± 0.57
Ω_m	$0.3055^{+0.0077}_{-0.0065}$	$0.3092^{+0.0067}_{-0.0061}$	0.2864 ± 0.0062	0.2804 ± 0.0061
S_8	0.827 ± 0.013	0.830 ± 0.012	0.822 ± 0.014	0.792 ± 0.015
$\Delta\chi^2_{\text{min}}$	-0.30	0.10	-8.54	-6.66
$\log B_{\text{M},\Lambda\text{CDM}}$	-3.1	-3.4	0	-1.2
Q_{DMAP}	...	5.51

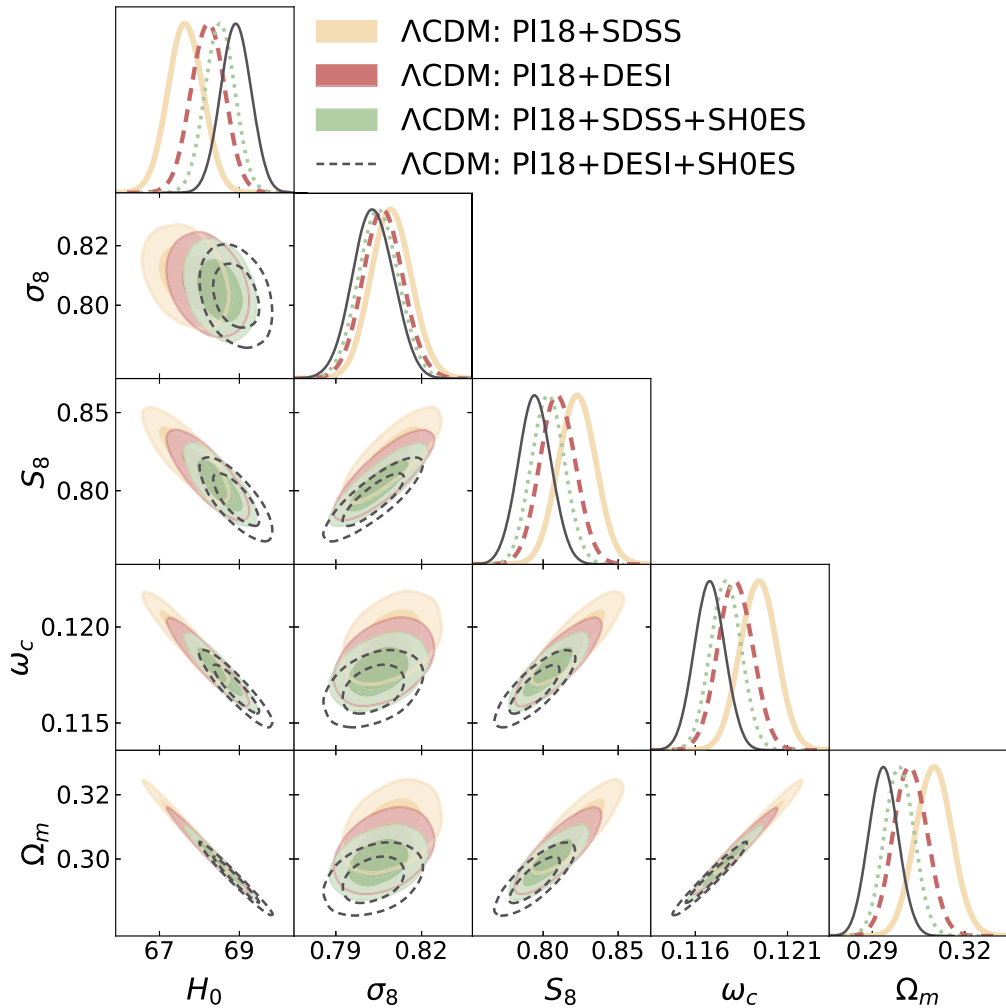


FIG. 7. Comparison of BAO data combinations for the Λ CDM model with SDSS and DESI.

[94,95], eBOSS quasars [96,97], and the combined BOSS + eBOSS Lyman- α autocorrelation and cross correlation [98]. Alongside the transverse measurements ($D_M(z)/r_d$), we incorporate radial BAO measurements ($D_H(z)/r_d$) from these datasets, as well as the angle-averaged measurement ($D_V(z)/r_d$) from the SDSS main galaxy sample [99,100]. Covariance matrices for these measurements are calculated following the approach described in [84]. Moreover, we combine these with the low- z BAO data gathered from 6dFGS at $z = 0.106$ [101] and SDSS DR7 MGS at $z = 0.15$ [99].

Tables IV and V summarize the results for the {PI18 + SDSS, PI18 + SDSS + SN, PI18 + SDSS + SH0ES} datasets in the context of the Λ CDM and the hybrid models, respectively, at 68% CL. Figures 7 and 8 provide contour plots comparing different dataset combinations using either DESI or SDSS BAO data for the Λ CDM and the hybrid models, respectively. Since SDSS favor larger Ω_m and smaller H_0 than DESI, the constraints on $1/\phi_i$ are stronger

than when using DESI, and the degeneracy with H_0 is less pronounced. This suggests that future DESI data will be of utmost importance with regard to the viability of this model to alleviate cosmic tensions.

APPENDIX B: RESULTS WHEN INCLUDING A_L

The phenomenological parameter A_L was introduced in [102] to account for various physical mechanisms that can influence the lensing amplitude of the CMB spectra by scaling the amplitude of the lensing trispectrum, effectively modeling the smoothing effects in the CMB temperature and polarization spectra. This parameter is defined such that the standard Λ CDM prediction corresponds to $A_L = 1$, while $A_L = 0$ represents a scenario where CMB lensing is completely ignored. By treating A_L as a free parameter, its value can be directly constrained by observational data, allowing for consistency tests with or deviations from the Λ CDM framework. From Planck temperature and polarization spectra, A_L deviates from 1 with a significance of

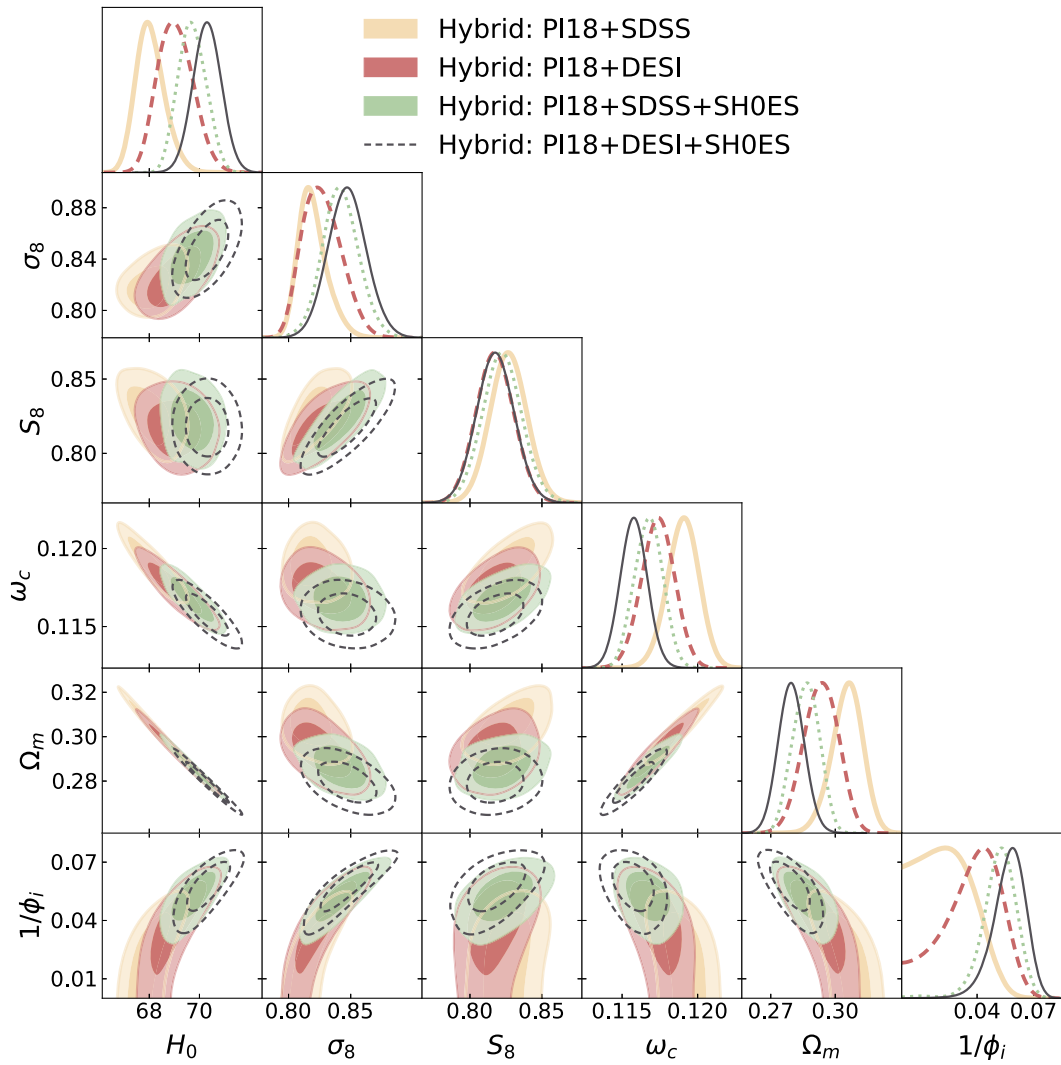


FIG. 8. Comparison of BAO data combinations for the hybrid model with SDSS and DESI.

about 2.8σ [103,104]. This issue can also be recast into an apparent preference for a closed universe in the Planck CMB data [105–108].

We explore the implication of the hybrid model for the dark sector for this A_L *anomaly*. This case is referred to as “PI18(A_L)” and we assume a flat prior range of $[0, 10]$ for A_L . We report our results for the case PI18(A_L)+DESI+SH0ES in the last column of Tables IV and V in the Λ CDM and hybrid models, respectively. We note that the combination of PI18(A_L) + DESI + SH0ES suggests a 4σ preference for $A_L > 1$ under Λ CDM. We caution that this data combination makes use of discrepant data sets (PI18 and SH0ES) and should thus be interpreted with a grain of salt. Under the hybrid model, the A_L parameter moves toward the Λ CDM value by $\sim 0.8\sigma$ but remains discrepant with $A_L = 1$ at the 3σ level.

APPENDIX C: PROFILE LIKELIHOOD AND χ^2 -VALUE TABLES

In this appendix, we provide a breakdown of the χ^2 fit for each model and data combination considered through a profile likelihood analysis performed with Procol [80]. In Table VI, we list the overall and individual dataset best-fit χ^2 values for the Λ CDM model and the hybrid model, as detailed in Sec. III A. In Fig. 9, we provide a comparison between the Bayesian posterior for the coupling parameter $1/\phi_i$ and the corresponding profile likelihood using the PI18 + DESI + SH0ES dataset. In Fig. 10, we show the breakdown of the χ^2 contribution from each experiment for the profile likelihood on H_0 in the hybrid model, for the combination of the experiments listed in the legend and described in Sec. III A.

TABLE VI. Best-fit χ^2 -values of overall and individual datasets considered in this work for the Λ CDM and hybrid models for various likelihood combinations.

Data	Model	Total χ^2	Pl18	DESI	SDSS	SN	SH0ES
Pl18	Λ CDM	2766.53	2766.53
	Hybrid	2766.55	2766.55
Pl18 + DESI	Λ CDM	2783.32	2768.82	14.50
	Hybrid	2780.51	2767.64	12.87
Pl18 + DESI + SN	Λ CDM	4195.78	2768.03	15.69	...	1412.06	...
	Hybrid	4194.54	2767.28	14.14	...	1413.12	...
Pl18 + DESI + SH0ES	Λ CDM	4105.02	2773.33	12.85	1318.84
	Hybrid	4092.07	2768.53	14.38	1309.16
Pl18 + SDSS	Λ CDM	2779.28	2767.03	...	12.25
	Hybrid	2778.87	2766.86	...	12.01
Pl18 + SN	Λ CDM	4177.11	2766.79	1410.32	...
	Hybrid	4177.03	2766.65	1410.38	...
Pl18 + SH0ES	Λ CDM	4091.93	2772.62	1319.31
	Hybrid	4075.63	2769.23	1306.40
Pl18 + SDSS + SN	Λ CDM	4190.30	2766.61	...	12.84	1410.85	...
	Hybrid	4190.27	2766.66	...	12.58	1411.03	...
Pl18 + SDSS + SH0ES	Λ CDM	4105.04	2770.40	...	12.72	...	1321.92
	Hybrid	4096.50	2768.35	...	15.71	...	1312.44

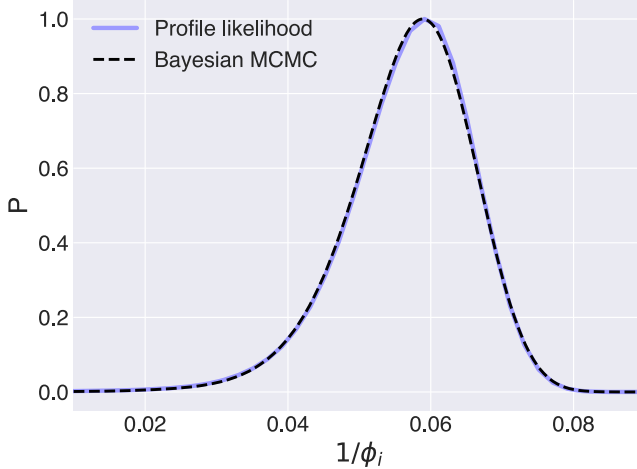


FIG. 9. Comparison between the Bayesian posterior for the coupling parameter $1/\phi_i$ and the corresponding profile likelihood using the Pl18 + DESI + SH0ES dataset as detailed in Sec. III A. Even though there is a potential prior volume effect related to the Λ CDM limit of the hybrid model ($1/\phi_i \rightarrow 0$), we see that the posteriors from the Bayesian MCMC analysis are reliable and do not appear to show a bias toward $1/\phi_i = 0$, as both likelihood curves are very similar and exhibit a maximum around the best-fit value of $1/\phi_i \simeq 0.06$.

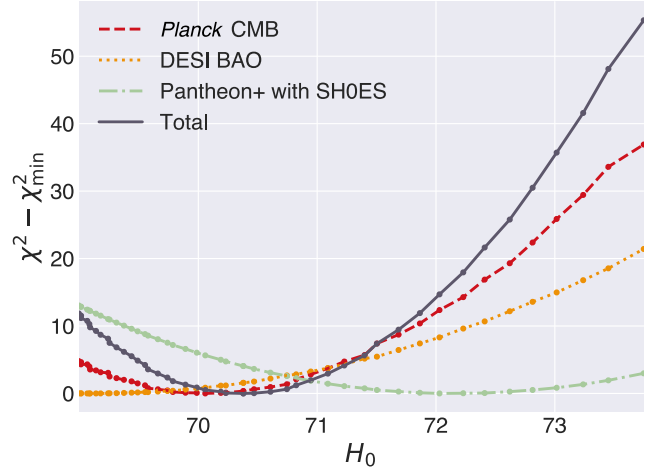


FIG. 10. Breakdown of the χ^2 contribution (normalized to its respective minimum) from each experiment for the profile likelihood on H_0 in the hybrid model, derived for the combination of the experiments listed in the legend and described in Sec. III A: the Pl18 dataset is shown in dashed red, DESI BAO in dotted yellow, and Pantheon + SN with the SH0ES calibration in dash-dotted green. The total $\chi^2 - \chi^2_{\min}$ is depicted in solid black and is the quantity optimized for producing the profile likelihood for this combination of data.

[1] P. J. E. Peebles, *Cosmology's Century: An Inside History of Our Modern Understanding of the Universe* (Princeton University Press, Princeton, NJ, 2022).

[2] Gianfranco Bertone, Dan Hooper, and Joseph Silk, Particle dark matter: Evidence, candidates and constraints, *Phys. Rep.* **405**, 279 (2005).

[3] David J. E. Marsh, Axion cosmology, *Phys. Rep.* **643**, 1 (2016).

[4] David J. E. Marsh, David Ellis, and Viraf M. Mehta, *Dark Matter: Evidence, Theory, and Constraints*, Princeton Series in Astrophysics (Princeton University Press, Princeton, NJ, 2024).

[5] Luca Amendola and Shinji Tsujikawa, *Dark Energy: Theory and Observations* (Cambridge University Press, Cambridge, England, 2015).

[6] Jerome Martin, Everything you always wanted to know about the cosmological constant problem (but were afraid to ask), *C.R. Phys.* **13**, 566 (2012).

[7] L. Verde, T. Treu, and A. G. Riess, Tensions between the early and the late universe, *Nat. Astron.* **3**, 891 (2019).

[8] Eleonora Di Valentino *et al.*, Snowmass2021—Letter of interest cosmology intertwined II: The Hubble constant tension, *Astropart. Phys.* **131**, 102605 (2021).

[9] Elcio Abdalla *et al.*, Cosmology intertwined: A review of the particle physics astrophysics, and cosmology associated with the cosmological tensions and anomalies, *J. High Energy Astrophys.* **34**, 49 (2022).

[10] Eleonora Di Valentino *et al.* (CosmoVerse Network Collaboration), The CosmoVerse white paper: Addressing observational tensions in cosmology with systematics and fundamental physics, *Phys. Dark Universe* **49**, 101965 (2025).

[11] Adam G. Riess *et al.*, A comprehensive measurement of the local value of the Hubble constant with $1 \text{ km s}^{-1} \text{ Mpc}^{-1}$ uncertainty from the Hubble space telescope and the SH0ES team, *Astrophys. J. Lett.* **934**, L7 (2022).

[12] Yukei S. Murakami, Adam G. Riess, Benjamin E. Stahl, W. D'Arcy Kenworthy, Dahne-More A. Pluck, Antonella Macorettta, Dillon Brout, David O. Jones, Dan M. Scolnic, and Alexei V. Filippenko, Leveraging SN Ia spectroscopic similarity to improve the measurement of H_0 , *J. Cosmol. Astropart. Phys.* **11** (2023) 046.

[13] Louise Breuval, Adam G. Riess, Stefano Casertano, Wenlong Yuan, Lucas M. Macri, Martino Romaniello, Yukei S. Murakami, Daniel Scolnic, Gagandeep S. Anand, and Igor Soszyński, Small magellanic cloud cepheids observed with the Hubble space telescope provide a new anchor for the SH0ES distance ladder, *Astrophys. J.* **973**, 30 (2024).

[14] Richard I. Anderson, Nolan W. Koblischke, and Laurent Eyer, Small-amplitude red giants elucidate the nature of the tip of the red giant branch as a standard candle, *Astrophys. J. Lett.* **963**, L43 (2024).

[15] D. Scolnic, A. G. Riess, J. Wu, S. Li, G. S. Anand, R. Beaton, S. Casertano, R. I. Anderson, S. Dhawan, and X. Ke, CATS: The Hubble constant from standardized TRGB and Type Ia supernova measurements, *Astrophys. J. Lett.* **954**, L31 (2023).

[16] Syed A. Uddin *et al.*, Carnegie supernova project I and II: Measurements of H_0 using cepheid, tip of the red giant branch, and surface brightness fluctuation distance calibration to type Ia supernovae, *Astrophys. J.* **970**, 72 (2024).

[17] Caroline D. Huang *et al.*, The mira distance to M101 and a 4% measurement of H_0 , *Astrophys. J.* **963**, 83 (2024).

[18] Siyang Li, Adam G. Riess, Stefano Casertano, Gagandeep S. Anand, Daniel M. Scolnic, Wenlong Yuan, Louise Breuval, and Caroline D. Huang, Reconnaissance with JWST of the J-region asymptotic giant branch in distance ladder galaxies: From irregular luminosity functions to approximation of the Hubble constant, *Astrophys. J.* **966**, 20 (2024).

[19] Wendy L. Freedman, Barry F. Madore, Taylor J. Hoyt, In Sung Jang, Abigail J. Lee, and Kayla A. Owens, Status report on the Chicago-Carnegie Hubble program (CCHP): Measurement of the Hubble constant using the Hubble and James webb space telescopes, *Astrophys. J.* **985**, 203 (2025).

[20] Adam G. Riess *et al.*, JWST validates HST distance measurements: Selection of supernova subsample explains differences in JWST estimates of local H_0 , *Astrophys. J.* **977**, 120 (2024).

[21] Christian Vogl *et al.*, No rungs attached: A distance-ladder free determination of the Hubble constant through type II supernova spectral modelling, *Astron. Astrophys.* **702**, A41 (2025).

[22] Daniel Scolnic *et al.*, The Hubble tension in our own backyard: DESI and the nearness of the coma cluster, *Astrophys. J. Lett.* **979**, L9 (2025).

[23] Khaled Said *et al.*, DESI peculiar velocity survey—fundamental plane, *Mon. Not. R. Astron. Soc.* **539**, 3627 (2025).

[24] Paula Boubel, Matthew Colless, Khaled Said, and Lister Staveley-Smith, An improved Tully–Fisher estimate of H_0 , *Mon. Not. R. Astron. Soc.* **533**, 1550 (2024).

[25] Daniel Scolnic, Paula Boubel, Jakob Byrne, Adam G. Riess, and Gagandeep S. Anand, Calibrating the Tully–Fisher relation to measure the Hubble constant, [arXiv:2412.08449](https://arxiv.org/abs/2412.08449).

[26] Siyang Li, Adam G. Riess, Daniel Scolnic, Stefano Casertano, and Gagandeep S. Anand, JAGB 2.0: Improved constraints on the J-region asymptotic giant branch–based Hubble constant from an expanded sample of JWST observations, *Astrophys. J.* **988**, 97 (2025).

[27] Joseph B. Jensen, John P. Blakeslee, Michele Cantiello, Mikaela Cowles, Gagandeep S. Anand, R. Brent Tully, Ehsan Kourkchi, and Gabriella Raimondo, The TRGB-SBF Project. III. Refining the HST surface brightness fluctuation distance scale calibration with JWST, *Astrophys. J.* **987**, 87 (2025).

[28] Adam G. Riess *et al.*, The perfect host: JWST cepheid observations in a background-free SN Ia host confirm no bias in Hubble-constant measurements, *Astrophys. J. Lett.* **992**, L34 (2025).

[29] Max J. B. Newman *et al.*, Tip of the red giant branch distances to NGC 1316, NGC 1380, NGC 1404, & NGC 4457: A pilot study of a parallel distance ladder using

type Ia supernovae in early-type host galaxies, [arXiv:2508.20023](https://arxiv.org/abs/2508.20023).

[30] N. Aghanim *et al.* (Planck Collaboration), Planck 2018 results. VI. Cosmological parameters, *Astron. Astrophys.* **641**, A6 (2020); **652**, C4(E) (2021).

[31] Thibaut Louis *et al.* (ACT Collaboration), The Atacama Cosmology Telescope: DR6 power spectra, likelihoods and Λ CDM parameters, *J. Cosmol. Astropart. Phys.* **11** (2025) 062.

[32] E. Camphuis *et al.* (SPT-3G Collaboration), SPT-3G D1: CMB temperature and polarization power spectra and cosmology from 2019 and 2020 observations of the SPT-3G Main field, [arXiv:2506.20707](https://arxiv.org/abs/2506.20707).

[33] Lloyd Knox and Marius Millea, Hubble constant Hunter's guide, *Phys. Rev. D* **101**, 043533 (2020).

[34] Karsten Jedamzik, Levon Pogosian, and Gong-Bo Zhao, Why reducing the cosmic sound horizon alone can not fully resolve the Hubble tension, *Commun. Phys.* **4**, 123 (2021).

[35] Nils Schöneberg, Guillermo Franco Abellán, Andrea Pérez Sánchez, Samuel J. Witte, Vivian Poulin, and Julien Lesgourgues, The H_0 Olympics: A fair ranking of proposed models, *Phys. Rep.* **984**, 1 (2022).

[36] Marc Kamionkowski and Adam G. Riess, The Hubble tension and early dark energy, *Annu. Rev. Nucl. Part. Sci.* **73**, 153 (2023).

[37] Licia Verde, Nils Schöneberg, and Héctor Gil-Marín, A tale of many H_0 , *Annu. Rev. Astron. Astrophys.* **62**, 287 (2024).

[38] Ali Rida Khalife, Maryam Bahrami Zanjani, Silvia Galli, Sven Günther, Julien Lesgourgues, and Karim Benabed, Review of Hubble tension solutions with new SH0ES and SPT-3G data, *J. Cosmol. Astropart. Phys.* **04** (2024) 059.

[39] *The Hubble Constant Tension*, edited by Eleonora Di Valentino and Dillon Brout, Springer Series in Astrophysics and Cosmology (Springer, New York, 2024).

[40] William Giarè, CMB anomalies, and the Hubble tension, [10.1007/978-99-0177-7_36](https://doi.org/10.1007/978-99-0177-7_36) (2023).

[41] Catherine Heymans *et al.*, KiDS-1000 cosmology: Multi-probe weak gravitational lensing and spectroscopic galaxy clustering constraints, *Astron. Astrophys.* **646**, A140 (2021).

[42] T. M. C. Abbott *et al.* (DES Collaboration), Dark energy survey year 3 results: Cosmological constraints from galaxy clustering and weak lensing, *Phys. Rev. D* **105**, 023520 (2022).

[43] Roohi Dalal *et al.*, Hyper Suprime-Cam Year 3 results: Cosmology from cosmic shear power spectra, *Phys. Rev. D* **108**, 123519 (2023).

[44] Eleonora Di Valentino *et al.*, Cosmology intertwined III: $f\sigma_8$ and S_8 , *Astropart. Phys.* **131**, 102604 (2021).

[45] Andrej Dvornik *et al.*, KiDS-1000: Combined halo-model cosmology constraints from galaxy abundance, galaxy clustering and galaxy-galaxy lensing, *Astron. Astrophys.* **675**, A189 (2023); **688**, C3(E) (2024).

[46] L. Faga *et al.* (DES Collaboration), Dark energy survey year 3 results: Cosmology from galaxy clustering and galaxy-galaxy lensing in harmonic space, *Mon. Not. R. Astron. Soc.* **536**, 1586 (2024).

[47] Joachim Harnois-Deraps *et al.*, KiDS-1000 and DES-Y1 combined: Cosmology from peak count statistics, *Mon. Not. R. Astron. Soc.* **534**, 3305 (2024).

[48] Leandros Perivolaropoulos and Foteini Skara, Challenges for Λ CDM: An update, *New Astron. Rev.* **95**, 101659 (2022).

[49] Eleonora Di Valentino, Olga Mena, Supriya Pan, Luca Visinelli, Weiqiang Yang, Alessandro Melchiorri, David F. Mota, Adam G. Riess, and Joseph Silk, In the realm of the Hubble tension—a review of solutions, *Classical Quantum Gravity* **38**, 153001 (2021).

[50] Carsten van de Bruck, Gaspard Poulot, and Elsa M. Teixeira, Scalar field dark matter and dark energy: A hybrid model for the dark sector, *J. Cosmol. Astropart. Phys.* **07** (2023) 019.

[51] A. G. Adame *et al.* (DESI Collaboration), DESI 2024 VI: Cosmological constraints from the measurements of baryon acoustic oscillations, *J. Cosmol. Astropart. Phys.* **02** (2025) 021.

[52] William Giarè, Dynamical dark energy beyond Planck? Constraints from multiple CMB probes, DESI BAO and Type-Ia supernovae, *Phys. Rev. D* **112**, 023508 (2025).

[53] Marina Cortês and Andrew R. Liddle, Interpreting DESI's evidence for evolving dark energy, *J. Cosmol. Astropart. Phys.* **12** (2024) 007.

[54] Vrund Patel, Amlan Chakraborty, and Luca Amendola, The prior dependence of the DESI results, [arXiv:2407.06586](https://arxiv.org/abs/2407.06586).

[55] William Giarè, Miguel A. Sabogal, Rafael C. Nunes, and Eleonora Di Valentino, Interacting dark energy after DESI baryon acoustic oscillation measurements, *Phys. Rev. Lett.* **133**, 251003 (2024).

[56] William Giarè, Mahdi Najafi, Supriya Pan, Eleonora Di Valentino, and Javad T. Firouzjaee, Robust preference for dynamical dark energy in DESI BAO and SN measurements, *J. Cosmol. Astropart. Phys.* **10** (2024) 035.

[57] Kim V. Berghaus, Joshua A. Kable, and Vivian Miranda, Quantifying scalar field dynamics with DESI 2024 Y1 BAO measurements, *Phys. Rev. D* **110**, 103524 (2024).

[58] George Efstathiou, Evolving dark energy or supernovae systematics?, *Mon. Not. R. Astron. Soc.* **538**, 875 (2025).

[59] Andrei D. Linde, Hybrid inflation, *Phys. Rev. D* **49**, 748 (1994).

[60] Subinoy Das, Pier Stefano Corasaniti, and Justin Khoury, Superacceleration as the signature of a dark sector interaction, *Phys. Rev. D* **73**, 083509 (2006).

[61] Carsten van de Bruck and Elsa M. Teixeira, Dark d-brane cosmology: From background evolution to cosmological perturbations, *Phys. Rev. D* **102**, 103503 (2020).

[62] Edmund J. Copeland, M. Sami, and Shinji Tsujikawa, Dynamics of dark energy, *Int. J. Mod. Phys. D* **15**, 1753 (2006).

[63] Julien Lesgourgues, The cosmic linear anisotropy solving system (CLASS) I: Overview, [arXiv:1104.2932](https://arxiv.org/abs/1104.2932).

[64] Diego Blas, Julien Lesgourgues, and Thomas Tram, The cosmic linear anisotropy solving system (CLASS). Part II: Approximation schemes, *J. Cosmol. Astropart. Phys.* **07** (2011) 034.

[65] Julien Lesgourgues, The cosmic linear anisotropy solving system (CLASS) III: Comparision with camb for lamb-dadm, [arXiv:1104.2934](https://arxiv.org/abs/1104.2934).

[66] Thejs Brinckmann and Julien Lesgourgues, MontePython 3: boosted MCMC sampler and other features, *Phys. Dark Universe* **24**, 100260 (2019).

[67] Benjamin Audren, Julien Lesgourgues, Karim Benabed, and Simon Prunet, Conservative constraints on early cosmology with MontePython, *J. Cosmol. Astropart. Phys.* **02** (2013) 001.

[68] Antony Lewis, Efficient sampling of fast and slow cosmological parameters, *Phys. Rev. D* **87**, 103529 (2013).

[69] Andrew Gelman and Donald B. Rubin, Inference from iterative simulation using multiple sequences, *Stat. Sci.* **7**, 457 (1992).

[70] Antony Lewis, GetDist: A Python package for analysing Monte Carlo samples, *J. Cosmol. Astropart. Phys.* **08** (2025) 025.

[71] N. Aghanim *et al.* (Planck Collaboration), Planck 2018 results. I. Overview and the cosmological legacy of Planck, *Astron. Astrophys.* **641**, A1 (2020).

[72] N. Aghanim *et al.* (Planck Collaboration), Planck 2018 results. V. CMB power spectra and likelihoods, *Astron. Astrophys.* **641**, A5 (2020).

[73] Erik Rosenberg, Steven Gratton, and George Efstathiou, CMB power spectra and cosmological parameters from Planck PR4 with CamSpec, *Mon. Not. R. Astron. Soc.* **517**, 4620 (2022).

[74] M. Tristram *et al.*, Cosmological parameters derived from the final Planck data release (PR4), *Astron. Astrophys.* **682**, A37 (2024).

[75] A. G. Adame *et al.* (DESI Collaboration), DESI 2024 III: Baryon acoustic oscillations from galaxies and quasars, *J. Cosmol. Astropart. Phys.* **04** (2025) 012.

[76] A. G. Adame *et al.* (DESI Collaboration), DESI 2024 IV: Baryon acoustic oscillations from the Lyman alpha forest, *J. Cosmol. Astropart. Phys.* **01** (2025) 124.

[77] Dan Scolnic *et al.*, The Pantheon + Analysis: The full data set and light-curve release, *Astrophys. J.* **938**, 113 (2022).

[78] Dillon Brout *et al.*, The Pantheon + Analysis: Cosmological Constraints, *Astrophys. J.* **938**, 110 (2022).

[79] Dillon Brout *et al.*, The Pantheon + Analysis: SuperCalfragilistic cross calibration, retrained SALT2 light-curve model, and calibration systematic uncertainty, *Astrophys. J.* **938**, 111 (2022).

[80] Tanvi Karwal, Yashvi Patel, Alexa Bartlett, Vivian Poulin, Tristan L. Smith, and Daniel N. Pfeffer, Procoli: Profiles of cosmological likelihoods, [arXiv:2401.14225](https://arxiv.org/abs/2401.14225).

[81] Alan Heavens, Yabebal Fantaye, Arrykrishna Mootoovaloo, Hans Eggers, Zafirah Hosenie, Steve Kroon, and Elena Sellentin, Marginal likelihoods from Monte Carlo Markov Chains, [arXiv:1704.03472](https://arxiv.org/abs/1704.03472).

[82] Alan Heavens, Yabebal Fantaye, Elena Sellentin, Hans Eggers, Zafirah Hosenie, Steve Kroon, and Arrykrishna Mootoovaloo, No evidence for extensions to the standard cosmological model, *Phys. Rev. Lett.* **119**, 101301 (2017).

[83] Marco Raveri and Wayne Hu, Concordance and discordance in cosmology, *Phys. Rev. D* **99**, 043506 (2019).

[84] Shadab Alam *et al.* (eBOSS Collaboration), Completed SDSS-IV extended Baryon Oscillation Spectroscopic Survey: Cosmological implications from two decades of spectroscopic surveys at the Apache Point Observatory, *Phys. Rev. D* **103**, 083533 (2021).

[85] Harold Jeffreys, *Theory of Probability* (Clarendon Press, Oxford, England, 1939).

[86] Marco Raveri, Resolving the Hubble tension at late times with dark energy, [arXiv:2309.06795](https://arxiv.org/abs/2309.06795).

[87] Michel Chevallier and David Polarski, Accelerating universes with scaling dark matter, *Int. J. Mod. Phys. D* **10**, 213 (2001).

[88] Eric V. Linder, Exploring the expansion history of the universe, *Phys. Rev. Lett.* **90**, 091301 (2003).

[89] Eoin Ó. Colgáin and M. M. Sheikh-Jabbari, DESI and SNe: Dynamical dark energy, Ω_m tension or systematics?, *Mon. Not. R. Astron. Soc.* **542**, L24 (2025).

[90] Suhail Dhawan, Brodie Popovic, and Ariel Goobar, The axis of systematic bias in SN^{Ia} cosmology and implications for DESI 2024 results, *Mon. Not. R. Astron. Soc.* **540**, 1626 (2025).

[91] Shadab Alam *et al.* (BOSS Collaboration), The clustering of galaxies in the completed SDSS-III Baryon Oscillation Spectroscopic Survey: Cosmological analysis of the DR12 galaxy sample, *Mon. Not. R. Astron. Soc.* **470**, 2617 (2017).

[92] Julian E. Bautista *et al.* (eBOSS Collaboration), The completed SDSS-IV extended Baryon Oscillation Spectroscopic Survey: Measurement of the BAO and growth rate of structure of the luminous red galaxy sample from the anisotropic correlation function between redshifts 0.6 and 1, *Mon. Not. R. Astron. Soc.* **500**, 736 (2020).

[93] Hector Gil-Marin *et al.* (eBOSS Collaboration), The completed SDSS-IV extended Baryon Oscillation Spectroscopic Survey: Measurement of the BAO and growth rate of structure of the luminous red galaxy sample from the anisotropic power spectrum between redshifts 0.6 and 1.0, *Mon. Not. R. Astron. Soc.* **498**, 2492 (2020).

[94] Amélie Tamone *et al.* (eBOSS Collaboration), The completed SDSS-IV extended Baryon Oscillation Spectroscopic Survey: Growth rate of structure measurement from anisotropic clustering analysis in configuration space between redshift 0.6 and 1.1 for the Emission Line Galaxy sample, *Mon. Not. R. Astron. Soc.* **499**, 5527 (2020).

[95] Arnaud de Mattia *et al.* (eBOSS Collaboration), The completed SDSS-IV extended Baryon Oscillation Spectroscopic Survey: Measurement of the BAO and growth rate of structure of the emission line galaxy sample from the anisotropic power spectrum between redshift 0.6 and 1.1, *Mon. Not. R. Astron. Soc.* **501**, 5616 (2021).

[96] Jiamin Hou *et al.* (eBOSS Collaboration), The completed SDSS-IV extended Baryon Oscillation Spectroscopic Survey: BAO and RSD measurements from anisotropic clustering analysis of the Quasar Sample in configuration space between redshift 0.8 and 2.2, *Mon. Not. R. Astron. Soc.* **500**, 1201 (2020).

[97] Richard Neveux *et al.* (eBOSS Collaboration), The completed SDSS-IV extended Baryon Oscillation Spectroscopic Survey: BAO and RSD measurements from the anisotropic power spectrum of the quasar sample between redshift 0.8 and 2.2, *Mon. Not. R. Astron. Soc.* **499**, 210 (2020).

[98] Helion du Mas des Bourboux *et al.* (eBOSS Collaboration), The completed SDSS-IV Extended Baryon Oscillation Spectroscopic Survey: Baryon acoustic oscillations with Ly α forests, *Astrophys. J.* **901**, 153 (2020).

[99] Ashley J. Ross, Lado Samushia, Cullan Howlett, Will J. Percival, Angela Burden, and Marc Manera, The clustering of the SDSS DR7 main Galaxy sample—I. A 4 per cent distance measure at $z = 0.15$, *Mon. Not. R. Astron. Soc.* **449**, 835 (2015).

[100] Cullan Howlett, Ashley Ross, Lado Samushia, Will Percival, and Marc Manera, The clustering of the SDSS main galaxy sample—II. Mock galaxy catalogues and a measurement of the growth of structure from redshift space distortions at $z = 0.15$, *Mon. Not. R. Astron. Soc.* **449**, 848 (2015).

[101] Florian Beutler, Chris Blake, Matthew Colless, D. Heath Jones, Lister Staveley-Smith, Lachlan Campbell, Quentin Parker, Will Saunders, and Fred Watson, The 6dF Galaxy Survey: Baryon acoustic oscillations and the local Hubble constant, *Mon. Not. R. Astron. Soc.* **416**, 3017 (2011).

[102] Erminia Calabrese, Anze Slosar, Alessandro Melchiorri, George F. Smoot, and Oliver Zahn, Cosmic microwave weak lensing data as a test for the dark universe, *Phys. Rev. D* **77**, 123531 (2008).

[103] Eleonora Di Valentino, Alessandro Melchiorri, and Joseph Silk, Cosmological hints of modified gravity?, *Phys. Rev. D* **93**, 023513 (2016).

[104] Fabrizio Renzi, Eleonora Di Valentino, and Alessandro Melchiorri, Cornering the Planck A_{lens} anomaly with future CMB data, *Phys. Rev. D* **97**, 123534 (2018).

[105] Will Handley, Curvature tension: Evidence for a closed universe, *Phys. Rev. D* **103**, L041301 (2021).

[106] Eleonora Di Valentino, Alessandro Melchiorri, and Joseph Silk, Planck evidence for a closed Universe and a possible crisis for cosmology, *Nat. Astron.* **4**, 196 (2019).

[107] George Efstathiou and Steven Gratton, The evidence for a spatially flat Universe, *Mon. Not. R. Astron. Soc.* **496**, L91 (2020).

[108] Eleonora Di Valentino, Alessandro Melchiorri, and Joseph Silk, Investigating cosmic discordance, *Astrophys. J. Lett.* **908**, L9 (2021).